SCIENCE CHINA Materials REVIEWS

mater.scichina.com link.springer.com

Published online 13 February 2019 | https://doi.org/10.1007/s40843-018-9398-1
Sci China Mater 2019, 62(6): 759–775

Phase engineering of two-dimensional transition metal dichalcogenides

Yao Xiao[1], Mengyue Zhou[2], Jinglu Liu[2], Jing Xu[2] and Lei Fu[1,2*]

ABSTRACT **Two-dimensional (2D) transition metal dichalcogenides (TMDs) have gained much attention in virtue of their various atomic configurations and band structures. Apart from those thermodynamically stable phases, plenty of metastable phases exhibit interesting properties. To obtain 2D TMDs with specific phases, it is important to develop phase engineering strategies including phase transition and phase-selective synthesis. Phase transition is a conventional method to transform one phase to another, while phase-selective synthesis means the direct fabrication of the target phases for 2D TMDs. In this review, we introduce the structures and stability of 2D TMDs with different phases. Then, we summarize the detailed processes and mechanism of the traditional phase transition strategies. Moreover, in view of the increasing demand of high-phase purity TMDs, we present the advanced phase-selective synthesis strategies. Finally, we underline the challenges and outlooks of phase engineering of 2D TMDs in two aspects—high phase purity and excellent controllability. This review may promote the development of controllable phase engineering for 2D TMDs and even other 2D materials toward both fundamental studies and practical applications.**

Keywords: phase engineering, transition metal dichalcogenides, phase transition, phase-selective synthesis

INTRODUCTION

Beyond graphene, transition metal dichalcogenides (TMDs) have become a series of outstanding two-dimensional (2D) materials for the variation of their structures and properties [1–10]. 2D TMDs with diverse band structures are essential to both fundamental research and applications. In detail, 2D TMDs with suitable bandgaps can be utilized for high-performance logic circuits and broadband photodetectors [1,11], and others exhibit novel physical properties including superconductivity, ferroelectricity, ferromagnetism and quantum spin Hall (QSH) effect [12–20]. Owing to the different symmetry, TMDs with different phases vary in the electron density of state (DOS) and charge distribution, as well as phonon DOS (PDOS), which directly affect their electrical, optical, magnetic, thermal and even mechanical properties [21–25].

Theoretical studies demonstrate a number of TMD structures with remarkable properties, and their stability varies greatly [26–29]. Some metastable phases are hardly obtained in the ambient condition. On the basis of close connection among TMD structures, stability and properties, it is vital to exploit effective pathways toward the specific phases. Therefore, phase engineering for TMDs has gained wide attention, which can open up a new territory for modulating the structure and properties of TMDs [30,31].

Here, in view of recent progress, we reviewed phase engineering of 2D TMDs. Initially, we introduced several types of TMD structures, and summarized their stability and properties. Then, we expounded phase engineering strategies which were classified into two types—phase transition and phase-selective synthesis, in accordance with the different process (Fig. 1). Specifically, phase transition is the transformation from one phase to another, where a stable TMD generally turns into a metastable one. Phase-selective synthesis focuses on the direct fabrication of high-purity phase TMDs or heterostructures rather than the transformation process. We presented the promoting factors and the corresponding feature and mechanism for the phase transition, including intercalation, charge transfer, external irradiation, thermal treatment and stress induction. For phase-selective synthesis, we analyzed the influence of different reaction conditions such as the precursor, temperature, atmosphere and extra assisted medium on the as-

[1] The Institute for Advanced Studies (IAS), Wuhan University, Wuhan 430072, China
[2] College of Chemistry and Molecular Sciences, Wuhan University, Wuhan 430072, China
* Corresponding author (email: leifu@whu.edu.cn)

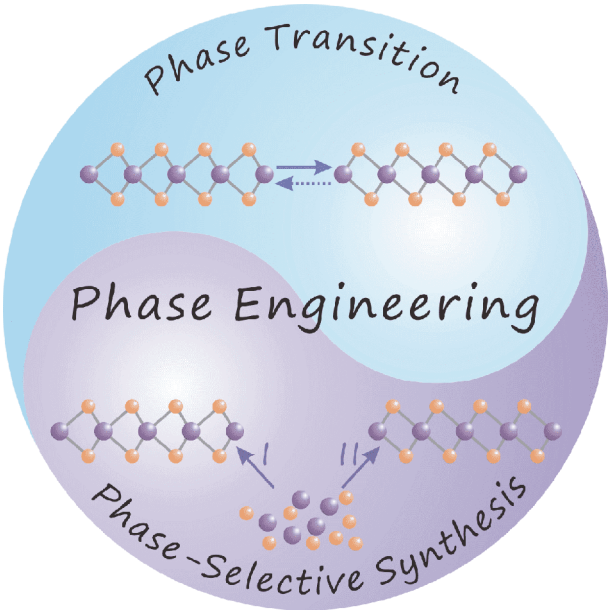

Figure 1 Schematic illustration of phase engineering of 2D TMDs.

synthesized 2D TMDs. Finally, we summarized the merits and demerits for both the phase transition and phase-selective synthesis strategies. We also pointed out the problems in phase engineering at present and the possible trend in the future. We believe that phase engineering of 2D TMDs is promising for the discovery of novel physical phenomena and high-performance devices.

STRUCTURES AND STABILITIES OF TMDs

With the variation of the oxidation states of transition metals, 2D TMDs exhibit diverse structures. According to the atomic configurations, monolayer 2D TMDs generally present two basic phases—the trigonal prismatic and the octahedral phases, referring to the 1H and 1T phase with D_{3h} and D_{3d} symmetry, respectively (Fig. 2a and b) [1,21]. In addition, 1T phase TMDs derive distorted structures (1T' and 1T'' phases) (Fig. 2c and d), according to the different distortions [32]. The different stacking arrangements of 1H phase layers result in 2H and 3R phases (Fig. 2e and f). Besides these polymorphs, the transformation from 1T' phase to T_d phase also derives from the symmetry change of stacked 1T' layers [2]. Different atomic configurations of TMDs originate from the different situation of the filling of d orbitals of transition metals. In addition to the different groups of transition metals, the stability of 2D TMDs is ascribed to the filling of d orbitals [21]. Therefore, 2D TMDs with different phases show the variations of thermodynamic stability [27]. Fig. 2g lists the layered TMDs together with the corresponding structures and stability. In detail, group IVB (d^0) and group VIII (d^6) TMDs only have octahedral structures. Most of group VIB (d^2) TMDs present trigonal prismatic phases, and group VB (d^1) TMDs could exhibit both trigonal prismatic and octahedral structures, whereas group VIIB (d^3) TMDs generally show distorted octahedral structures. Taking Mo- and W-based TMDs as

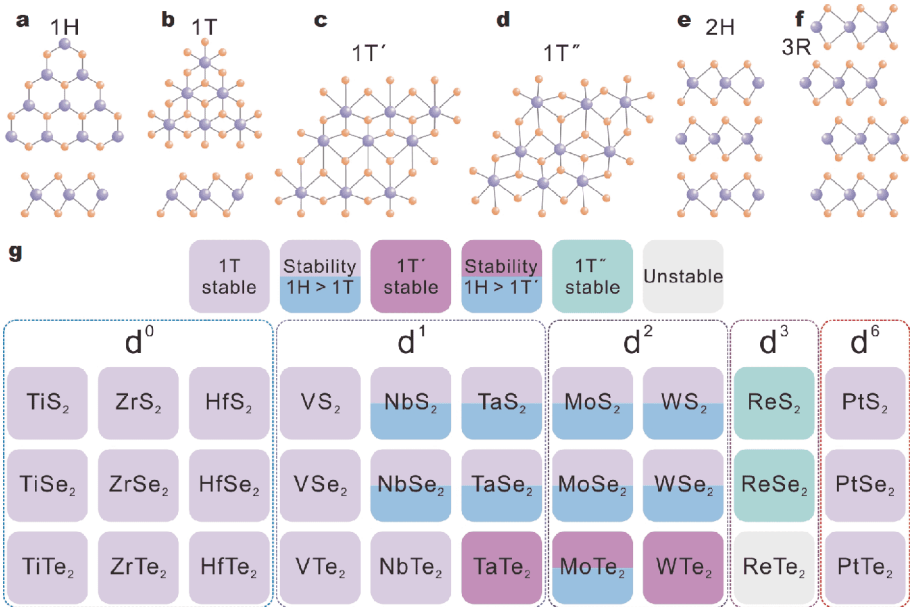

Figure 2 Structures and stability of 2D TMDs. (a–f) Different phases of 2D TMDs: (a) 1H, (b) 1T, (c) 1T', (d) 1T'', (e) 2H and (f) 3R phases. (g) Summary of structures and stability of 2D TMDs including group IVB, VB, VIB, VIIB and VIII.

examples, the trigonal prismatic phases of (Mo,W)S_2, (Mo,W)Se_2 and $MoTe_2$ are much more stable than the octahedral ones of those, whereas the situation is completely opposite for WTe_2, in accordance with the ground state energy differences [33]. It means that WTe_2 tends to become a 1T' phase rather than a 1H phase at the ground state.

Variation of 2D TMD phases provides a diversity of interesting properties for fundamental research and further applications [1,2]. Table 1 classifies 2D TMDs into semiconductors, metals and semimetals, according to their band structures. Especially for those semiconducting ones, their bandgaps are also listed. Moreover, owing to the special physical properties, metastable phases of TMDs have gained much attention. For instance, the 1T-MoS_2 possesses superconductivity, magnetism, ferroelectricity and memristive behavior [34], which are potential for electronics, catalysis and energy storage. To obtain those metastable phases or construct the polymorphic heterostructures, giant efforts have been devoted to phase engineering of 2D TMDs, including phase transition and phase-selective synthesis.

STRATEGIES OF PHASE TRANSITION FOR 2D TMDs

The physical and chemical properties of 2D materials are dominated by their structures [70,71], and subtle structural changes could generate different properties [72–76]. Although the synthesis of 2D TMDs with stable phases has been mature, the direct fabrication of their metastable phases remains challenging. As a typical route, the phase transition is regarded as an efficient approach to obtain these metastable phases. Here, various phase transition strategies as well as their mechanisms are expounded.

Intercalation

Intercalation is one of the most common methods for the phase transition of 2D TMDs. Early in 1983, Haering *et al.* [70] reported that Li intercalation in 2H-MoS_2 induced a structural transformation, in which Mo coordination transformed from 2H to 1T phase. Different from a rapid increase of the electron energy of MoS_2 from 2H-MoS_2 to 2H-$LiMoS_2$ [77], the phase transition is attributed to the small increase in 1T-$LiMoS_2$ without an energy gap. Besides, the transformation from 2H-$MoSe_2$ to 1T-$LiMoSe_2$ can also be realized [70]. It is noteworthy that Li-intercalation is generally driven by external assistance, such as ball milling [78], electrochemical process [79,80], and sonication [81,82], which can help to

Table 1 Electrical properties of 2D TMDs of different phases

TMD	Phase	Electronic characteristics	Ref.
TiS_2	1T	Metallicity	[35]
$TiSe_2$	1T	Metallicity	[36]
$TiTe_2$	1T	Metallicity	[37]
ZrS_2	1T	Semiconducting (1.4 eV)	[38]
$ZrSe_2$	1T	Semiconducting (0.95 eV)	[39]
$ZrTe_2$	1T	Dirac semimetallicity	[40]
HfS_2	1T	Semiconducting (1.45 eV)	[41]
$HfSe_2$	1T	Semiconducting (1.13 eV)	[39]
$HfTe_2$	1T	Semimetallicity	[42]
VS_2	1T	Semiconducting (0.3 eV, 2–3 layers)	[43]
		Metallicity (>8 layers)	[44]
VSe_2	1T	Metallicity	[18]
VTe_2	1T	Metallicity	[45]
NbS_2	2H	Metallicity	[46]
	1T	Metallicity	[47]
$NbSe_2$	2H	Metallicity	[16]
	1T	Metallicity	[48]
$NbTe_2$	1T	Metallicity	[45]
TaS_2	2H	Metallicity	[49]
	1T	Metallicity	[50]
$TaSe_2$	2H	Metallicity	[51]
	1T	Metallicity	[52]
$TaTe_2$	1T'	Metallicity	[45]
MoS_2	2H	Semiconducting (1.85 eV)	[53]
	1T	Metallicity	[54]
$MoSe_2$	2H	Semiconducting (1.55 eV)	[55]
	1T	Metallicity	[56]
$MoTe_2$	2H	Semiconducting (1.1 eV)	[57]
	1T'	Metallicity	[58]
	T_d	Weyl semimetallicity	[59]
WS_2	2H	Semiconducting (2.02 eV)	[60]
	1T	Metallicity	[25]
WSe_2	2H	Semiconducting (1.7 eV)	[61]
	1T	Metallicity	[62]
WTe_2	1T'	Semimetallicity	[63]
	T_d	Weyl semimetallicity	[64]
ReS_2	1T''	Semiconducting (1.43 eV)	[65]
$ReSe_2$	1T''	Semiconducting (1.22 eV)	[66]
PtS_2	1T	Semiconducting (1.75 eV)	[67]
$PtSe_2$	1T	Semiconducting (1.13 eV)	[68]
$PtTe_2$	1T	Dirac semimetallicity	[69]

overcome the energy barrier of phase transition. Detailed phase transition mechanism and the intercalation stability have been widely studied. In general, H-MoS_2 changes into T-$LiMoS_2$ during the early lithiation on account of the unusual interaction of intrinsic doping and electron-phonon coupling. In case of deep lithiation, T-$LiMoS_2$ would be transformed into Li_2S and Mo clusters [83]. In a word, the lithiation process should be controlled, otherwise the materials may be degraded. Besides the lithiation process, the environmental factors have impacts on the stability of Li-intercalated TMDs. To avoid such unexpected reversion from the as-obtained 1T to the 2H phase [84–87], a thermal activated hydrogenation method is put forward to substitute LiH for Li [88]. Furthermore, the phase transition induced by intercalation also depends on the thickness of MoS_2, because the layer number affects both the energy difference between 2H- and 1T'-MoS_2 and the critical injected electron concentrations [89].

In situ characterization and theoretical calculation uncover the detailed processes. Bai *et al.* [90] studied the mechanism of dynamic electrochemical lithiated MoS_2 processes by *in situ* high-resolution transmission electron microscopy (HRTEM). The phase transition of MoS_2 is confirmed according to the polytype superlattice with a Li ion occupying the interlayer S–S tetrahedron site. During the Li intercalation, the electron transfer from the intercalant to TMDs leads to the electron density increase of the d orbital of the transition metals, which induces the destabilization of the 2H phase and accelerates the phase transition to the metallic 1T phase. Jena *et al.* [91] generalized the probable pathways for the phase transition of MoS_2 (Fig. 3a). At first, the trigonal prismatic H-MoS_2 starts to change into the octahedral coordinated O-MoS_2 (as the 1T phase mentioned above) when Li concentration reaches 20%. Then, as the concentration of Li increases to 100%, O-MoS_2 becomes more stable, and the atomic configuration converts from zigzag chains to "diamond chains" to ultimately form the stable DT-MoS_2 (as the aforementioned 1T'' phase). Next, DT-MoS_2 turns into ZT-MoS_2 (equivalent to the 1T' phase), when all Li atoms are removed from the system. Finally, ZT-MoS_2 converts back to the original H-MoS_2 by heating or aging. The pathways contribute to further understanding of the phase transition *via* Li intercalation.

Other intercalants including Na, K, and ammonium ions have been employed to achieve the TMD phase transition [92–95]. It is demonstrated that appropriate intercalant concentration results in the phase transition, whereas the excessive concentration would lead to the structural degradation [92]. Distinct from alkali metal intercalants, the intercalated ammonium ions can stabilize the 1T-MoS_2 and 1T-WS_2 [94,95], which may innovate the phase transition conventionally triggered by alkali metal intercalation.

In summary, intercalation is a general means of the phase transition of 2D TMDs, whose stability may rely on the intercalation extent or the environment. Additionally, more efficient and specific intercalation methods still remain to be explored.

Charge transfer

In consideration of the different splitting conditions of d orbitals in different phases of 2D TMDs, charge transfer which tends to take place in the external electrical field or in the interfaces between materials is utilized to change the d orbital arrangements and induce the phase transition of 2D TMDs [21]. Promisingly, charge transfer can be nondestructive for the phase transition of 2D TMDs.

Electrostatic doping

Electrostatic doping is recognized as a damage-free strategy, which refers to the charge injection from an external electrostatic field. As theoretically predicted, the phase stability can be directly affected by external charge transfer [96], which is ascribed to the total energy difference of TMD phases associated with the charge density. Therefore, it is feasible to achieve the TMD phase transition by using the electrostatic gating devices. Reed *et al.* [96] discovered the imposed gate voltages serving as promoters through simulation. They demonstrated that the alteration of electronic chemical potential or carrier density can induce the phase transition of monolayer TMDs. On the basis of the prediction, Zhang *et al.* [97] achieved reversible phase transition between 2H and 1T' phases of monolayer $MoTe_2$ by imposing and withdrawing the electrostatic doping in the gating device (Fig. 3b). To confirm the components of the 1T' and 2H phases, they fitted the relative Raman mixture with Lorentz model. The relative content of the two phases was expressed by correlation Raman peak intensity ratio. The hysteretic loop of the gate-dependent Raman intensity ratios (Fig. 3c) indicates the reversible phase transition as the continuously decrease and increase of the gate voltage. In detail, Raman intensity ratio, $F=A_g(1T')/(A_1'(2H)+A_g(1T'))$, reflects the ratio of the phase transition, where $A_g(1T')$ and $A_1'(2H)$ refer to the Raman intensity of A_g mode of 1T'-$MoTe_2$ and A_1' mode of the 2H-$MoTe_2$, respectively. Along the forward sweeping, the

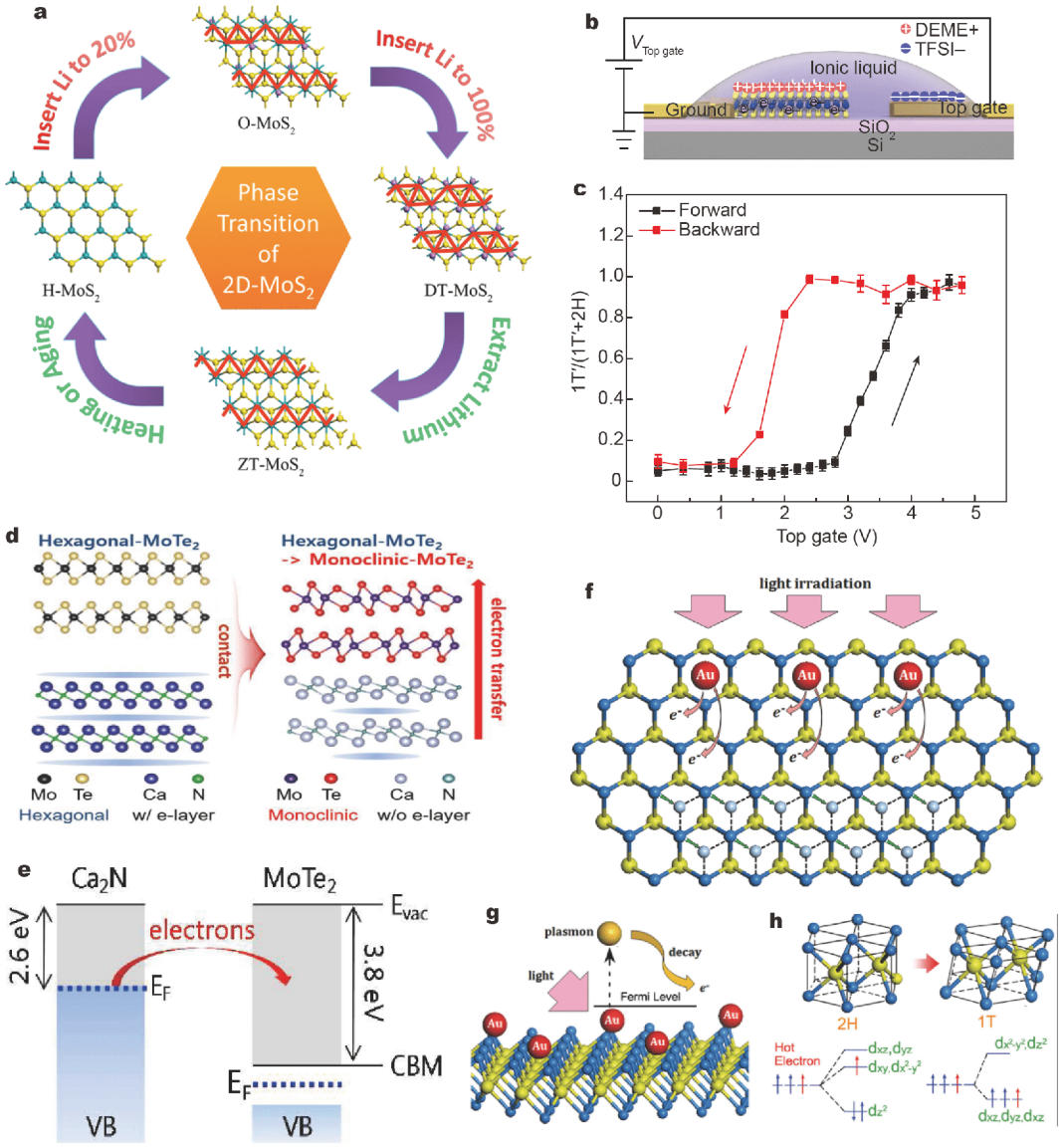

Figure 3 The phase transition of TMDs achieved by intercalation and charge transfer. (a) Possible paths of structural phase changes as lithium is intercalated in or extracted from MoS_2 monolayer. Reproduced with permission from Ref. [91]. Copyright 2014, American Chemical Society. (b) Schematic illustration of the phase transition of exfoliated monolayer $MoTe_2$ driven by electrostatic doping in a gating device. (c) Gate-dependent Raman intensity ratios F (y axis) of $MoTe_2$, showing a hysteresis loop with 1.8 V width under an electrical field scan. The red and black curves show decreasing and increasing gate voltage, respectively. Reproduced with permission from Ref. [97]. Copyright 2017, Springer Nature. (d) Schematic illustration of the phase transition of $MoTe_2$ *via* interface electron transfer, when it is vertically contacted with $[Ca_2N]^+ \cdot e^-$. (e) Band alignment of $MoTe_2$ and $[Ca_2N]^+ \cdot e^-$, indication the electron transfer in the interface. Reproduced with permission from Ref. [98]. Copyright 2017, American Chemical Society. (f–h) Schematic illustrations of plasmonic hot electron generated from Au induced phase transition of MoS_2 from 2H to 1T phase. Reproduced with permission from Ref. [99]. Copyright 2014, Wiley.

phase transition from 2H to 1T' phase begins at the gate voltage of 2.8 V, and it reaches the complete transformation at 3.8 V. When the gate voltage is swept backwards, the 2H phase starts to reappear at the gate voltage of 2.4 V and recovers completely at 1.2 V. Moreover, the phase transition occurs uniformly across the entire monolayer without obvious morphologic changes. Electrostatic doping can provide a versatile platform to study new topological phases. Dynamically controlled phase transition in 2D TMDs exhibits promising prospects in phase-

change electronics.

Interface electron transfer

In addition to charge injection *via* electrostatic doping, interface electron transfer also enables the phase transition by virtue of the charge transfer of different band alignments in contacting materials. Some materials, such as electrides and metals, take full advantage of free electrons to achieve the phase transition. Kim *et al.* [98] reported that the phase transition was triggered by the charge transfer, when $MoTe_2$ was contacted with the single-crystalline 2D $[Ca_2N]^+ \cdot e^-$ owning a low work function of ~2.6 eV (Fig. 3d). The first-principles calculations show that the interface electron transfer is driven by the energy difference (~1.2 eV) between the conduction band minimum (CBM) of 2H-$MoTe_2$ and the Fermi level of $[Ca_2N]^+ \cdot e^-$, as shown in Fig. 3e. It is simulated that a strong electron doping happens after the contact of two materials, where the Fermi level of $MoTe_2$ shifts 0.15 eV above the CBM. The strategy may be potential for constructing semiconductor-metal junctions toward high-performance electronics. It is speculated that suitable electron donors contacting with TMDs can induce the phase transition. Fang *et al.* [99] demonstrated that hot electrons produced by plasmon excitation in Au nanospheres (Fig. 3f) are able to induce a transient reversible phase transition (Fig. 3g). The hot electrons can be effectively transferred to MoS_2 monolayer, because of the low Schottky barrier (0.8 eV) between Au and MoS_2. In terms of crystal field theory, the Mo 4d orbitals split into three energy levels in 2H-MoS_2 or two levels in 1T-MoS_2, respectively [100,101]. Different from the unoccupied orbitals lying in the high-energy levels in 2H-MoS_2, there is an unoccupied orbital in the low-energy level in 1T-MoS_2, in which the hot electrons tend to fill to stabilize the 1T phase (Fig. 3h). Meanwhile, deposited Au can also result in a local slide of top S plane due to the interaction between MoS_2 and Au, which can weaken the bonding of top Mo–S and further lead to a destabilization of the structure to promote the phase transition [99,102].

To sum up, charge transfer, including electrostatic doping and interface electron transfer, plays an important role in the phase transition of TMDs for its damage-free process. Additionally, atomic doping can modulate the DOS of TMDs to induce the charge transfer, so it may be used in the phase transition of TMDs. Nb-doping can induce structural transition from 2H to 3R stacking in MoS_2 due to the lower total energy of Nb-doped 3R than that of Nb-doped 2H, which can be ascribed to free-carrier screening of holes residing in the d_{z^2} bands of Nb-doped MoS_2 [103,104]. Nevertheless, in consideration of the transformation of intrinsic properties, atomic doping is not very appropriate for the nondestructive phase transition.

External irradiation

External irradiation offers high-energy particles for the phase transition, including plasma [99,105], electron beam [102] and laser [106]. Here we review the detailed operation and the corresponding mechanism of the external irradiation strategies.

Plasma

Plasma treatment is a clean and scalable approach to phase transition owing to the high kinetic energy inducing the lateral sliding. However, it has also been reported that some vacancies are likely to occur during the plasma treating process [107,108]. Zhu *et al.* [105] reported a new phase transition way of Ar-plasma treatment being used to activate the 2H→1T phase transition. As shown in Fig. 4a, an inductively coupled plasma generated by dispersing a 20 W radio frequency (RF) power at the entrance of a quartz tube furnace using an RF (13.56 MHz) coil is applied to the as-grown MoS_2. It has been calculated that the kinetic energy of Ar ions is tuned well below the level where etching could occur but is sufficient to wrench the S–Mo bond to induce the lateral sliding of top S-layer. As shown in Fig. 4b, after inducing the phase transition, there are three weak but distinct new peaks J_1 (167 cm^{-1}), J_2 (227 cm^{-1}) and J_3 (334 cm^{-1}) appearing, which is in good agreement with the signature of the monolayer 1T-MoS_2 (inset of Fig. 4b). To sum up, plasma treating can open up a novel route for phase engineering in 2D TMDs, but it still needs further development in the controllability.

Electron beam

Electron-beam irradiation is an efficient method to achieve the phase transition, ascribing to high-energy-induced lattice reconstruction. Lin *et al.* [102] introduced the transformation from 2H to 1T of a single layer of MoS_2 under electron-beam irradiation. The 2H phase converts into a new phase by forming two band-like structures with an angle of 60°. Each stripe consists of three to four constricted MoS_2 zigzag chains (α in Fig. 4d) with decreased distance between two Mo atoms, at the intersection of which the over packed atoms trigger the formation of 1T phase to release the stress. With continuous electron-beam scanning, the 1T phase domain progressively forms a triangular shape, and at

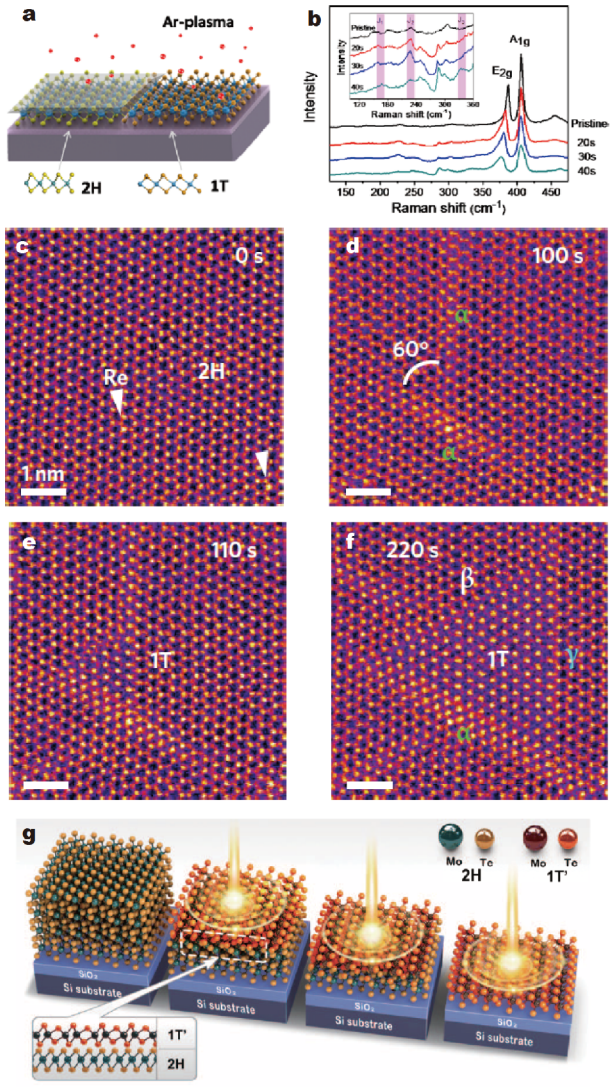

Figure 4 Phase transition induced by external irradiation. (a) Schematic representation of the plasma treatment process. (b) Time-dependent Raman spectra of monolayer MoS_2 and plasma-treated MoS_2. Reproduced with permission from Ref. [105]. Copyright 2017, American Chemical Society. (c–f) Atomic movements during 2H→1T phase transformation in the monolayer MoS_2 under electron beam irradiation. Reproduced with permission from Ref. [102]. Copyright 2014, Springer Nature. (g) Schematic representation of the laser-irradiation process. Reproduced with permission from Ref. [106]. Copyright 2015, the American Association for the Advancement of Science.

the same time as two new phase boundaries denoted as β and γ show two new atomic arrangements (Fig. 4c–f). Thus, the electron beam can be applied to intentionally induce the phase transition in a target area with a predetermined size toward specific nanoelectronics.

Laser

Laser irradiation, regarded as the high-energy photon beam, can achieve the phase transition without unexpected doping impurities. Cho *et al.* [106] designed a kind of local polymorph engineering, that is, they drove the phase transition from the 2H to 1T' phase in $MoTe_2$ *via* laser irradiation in a selected area. The researchers have confirmed that the top layer initially experienced the phase transition with the thinning effect, as shown in Fig. 4g, whereas the reverse phase transition was not observed by laser irradiating even with a higher energy or intensity of the laser.

Generally, these three techniques are facile to realize the controlled phase transition, due to the controllability of plasma, electron beam and laser. Nevertheless, high energy particles tend to bring some damage to the sample. Moreover, it is also worth mentioning that external irradiation may offer the patternable phase transition in the future, which is promising to be extended to industrial applications.

Thermal treatment

Thermal treatment is identified as one of the most convenient strategies, for its excellent controllability of the phase transition at different temperatures according to phase diagrams. The phase transition can easily occur with the frequent vibrations of atoms and the formations of new chemical bonds at a high temperature. Lee *et al.* [109] reported the synthesis of 2H- and 1T'-$MoTe_2$ in a two-zone chemical vapor deposition (CVD) system. At first, they obtained large-scale 2H-$MoTe_2$ *via* slow tellurization methods. In Fig. 5a, during the slow tellurization, the 1T'-$MoTe_2$ initially took place in the top region followed by the gradual transformation into 2H-$MoTe_2$. The researchers also presented that the reverse phase transition could occur by further tellurization or annealing rapidly. Kim *et al.* [110] obtained 2H- and 1T'-$MoTe_2$ *via* the flux method. As the phase diagram shown in Fig. 5b, the engineering of single crystalline 2H- and 1T'-$MoTe_2$ can be realized. In the phase diagram (Fig. 5b left), the 2H phase starts to convert into the stable 1T' phase at temperatures higher than 500°C (Fig. 5b right). Besides, the 2H phase can recover as it slowly cools with a new mixed phase appearing in a temperature range between 500 and 820°C, which illustrates the reversible structural phase transition. 2H phase can be obtained by slow cooling from 900°C to room temperature, while 1T' phase can be synthesized by quenching or rapid cooling process. *In situ* variable-temperature X-ray diffraction (XRD) patterns are

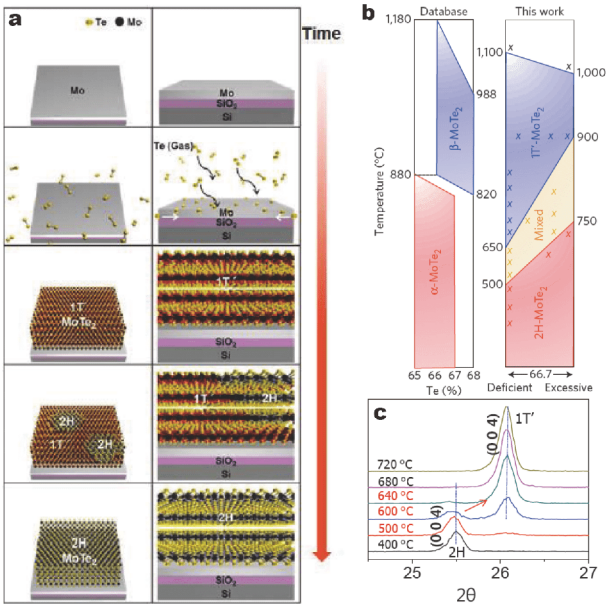

Figure 5 Phase transition induced by thermal treatment. (a) Schematic illustrations of the growth of 2H-$MoTe_2$ and the phase transition from 2H to 1T' phase. Reproduced with permission from Ref. [109]. Copyright 2015, American Chemical Society. (b) Phase diagram of $MoTe_2$. (c) *In situ* XRD results of $MoTe_2$ at different thermal treatment temperatures. Reproduced with permission from Ref. [110]. Copyright 2015, Springer Nature.

presented in Fig. 5c, which also proves that the structural phase transition begins at 500°C until the 2H-$MoTe_2$ completely transforms into 1T'-$MoTe_2$ at 680°C. Besides, it is also reported that group VB TMDs such as TaS_2 can realize phase transition by this approach. Wang *et al.* [111] found the 1T→2H polymorph transition on the surface of bulk-TaS_2 by thermal annealing because of the thermally induced relaxation derived from larger freedom for atom displacement. Although thermal methods are very efficient and convenient, the biggest problem lies in the precise control of the conditions and transition process, which might cause many limits especially in the applications of the few-layer materials.

Stress induction

Stress induction, which utilizes mechanical force to change the lattice structure of TMDs, provides another viable strategy for the phase transition. It is mainly realized by two different methods: tensile strain and hydrostatic pressure. The former realizes the transition *via* interlayer atomic plane gliding, while the latter distorts the lattice structure mechanically. Duerloo *et al.* [33] demonstrated that an equibiaxial tensile strain of 10%–15% was needed to achieve the phase transition for most of TMDs, among which it was the easiest to achieve in the case of $MoTe_2$ through a tensile strain less than 1.5%. Experimentally, Lee *et al.* [112] proposed a method to enable a reversible phase transition for $MoTe_2$ with a tensile strain exerted by an atomic force microscope (AFM) tip. As a function of forces, the system resistance changes by nearly four orders of magnitude, suggesting that $MoTe_2$ experiences the phase transition from semiconducting 2H phase to metallic 1T' phase under the tensile strain. Fully reversible transformation occurs after the release of strain. According to the force-temperature phase diagram in Fig. 6b, tensile strain can induce the phase transition at a certain temperature, and the needed strain becomes smaller as the temperature increases. The tensile strain may also induce the phase transition for other TMDs with underlying effects in addition to heat (e.g., electric fields and chemical doping).

It seems like a compressive stress to exert hydrostatic pressure on TMDs to induce the phase transition. Akinwande *et al.* [113] used a diamond anvil cell (DAC) to exert a uniform hydrostatic pressure on the MoS_2. As shown in Fig. 6c, it is revealed by theoretical calculation that the bandgap of the 2H-MoS_2 monolayer first increases until it reaches the peak as the applied pressure increases. Above the critical pressure, the bandgap gradually reduces, and finally the metallization of 2H-MoS_2 is predicted to be achieved at about 68 GPa. In addition, it is found that interlayer interactions play a significant role in the phase transition. That is, pressure acquired to achieve transition decreases as the layer number increases (Fig. 6d).

Though tensile strain applied by AFM can achieve the phase transition, it holds a notable feature that a phase reversal will occur after strain release, and thus it is unrealistic to obtain stable 1T'-TMDs by this method. Nevertheless, it is possible to be applied in the development of biological and optical sensors, on account of environmentally sensitive electrical property changes owing to the phase transition. Producing large hydrostatic pressure through DAC also faces the challenge to reach such high pressure, which hinders the practical application of the stress-induced phase transition.

Others

Besides intercalation, charge transfer, external irradiation, thermal treatment and stress induction, there are still many other methods of phase engineering. Xu *et al.* [73] utilized supercritical CO_2 in the intermediate layer of the as-exfoliated MoS_2 film to partially convert the 2H-MoS_2 nanosheets into the 1T phase and form lattice-matched

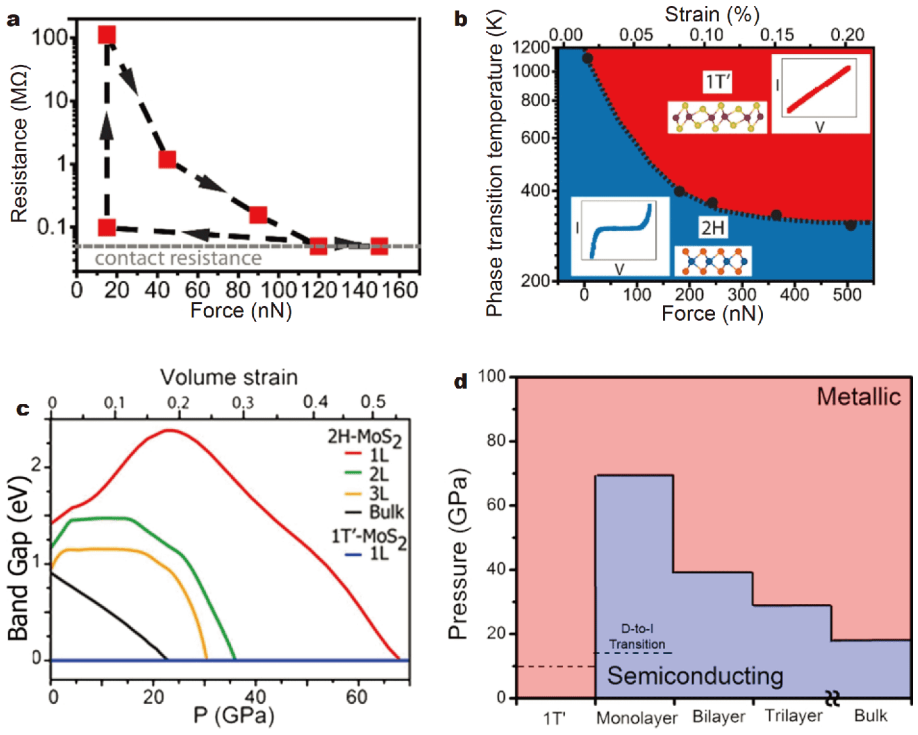

Figure 6 Phase transition achieved *via* stress induction. (a) Resistance plots of $MoTe_2$ with different tensile forces applied. The arrows show the reversible metallization of 2H-$MoTe_2$. (b) Phase diagram as a function of phase transition temperature and the tensile force. Insets show the structures and electrical properties of different phase $MoTe_2$. Reproduced with permission from Ref. [112]. Copyright 2016, American Chemical Society. (c) Bandgap changes as a function of hydrostatic pressure of 2H- and 1T-MoS_2 with different layer numbers. (d) Electrical characteristics of 2H- and 1T-MoS_2 with different layer numbers when the hydrostatic pressure changes. Reproduced with permission from Ref. [113]. Copyright 2015, American Chemical Society.

heterojunction. Moreover, the available conductivity of the 1T phase and the extended life of photogenerated electrons make such tailored MoS_2 perform high catalytic activity for water splitting. Besides, Chhowalla *et al.* [114] introduced the covalent functionalization of TMDs which relied on the electron transfer between the electron-rich metallic 1T phase and the covalent functional groups of an organohalide reactant instead of defect engineering. The reactions between amide and methyl moieties (from organoiodide precursors) successfully applied to MoS_2, WS_2 and $MoSe_2$ make the properties of the 1T phase transform from metallic to semiconducting. These special methods make it possible to combine the phase transition with solution surroundings, which may be applied in catalysis and sensing. Besides, as for alloyed phase heterostructures, there are still some approaches to partial phase transformation. Huang *et al.* [115] successfully obtained alloyed $Mo_xW_{1-x}S_2$ nanosheets by liquid-phase preparation and controlled the 1T concentration by altering the reaction temperature. They finally observed that a mixed 1T/2H phase $Mo_xW_{1-x}S_2$ with a 1T concentration of ~60% presented the best performance towards hydrogen evolution reaction (HER).

PHASE-SELECTIVE SYNTHESIS OF 2D TMDs

2D TMDs with different phases, especially for the metastable ones, can be effectively obtained through the aforementioned phase transition strategies, including intercalation, charge transfer, external irradiation, thermal treatment and stress induction. Despite the fact that the target phase of 2D TMDs can be efficiently and controllably gained *via* the phase transition, there are still some shortcomings. 1) The as-obtained phases may not keep stable after withdrawing the external factors for the phase transition, so they would be transformed reversibly to the original phases. 2) Atomic vacancies induced by high external energy for the phase transition would lead to the unexpected property modulation, as well as chemical doping originating from intercalation. Therefore, it is urgent to develop controllable fabrication strategies for high phase-purity TMDs. Recently, phase-

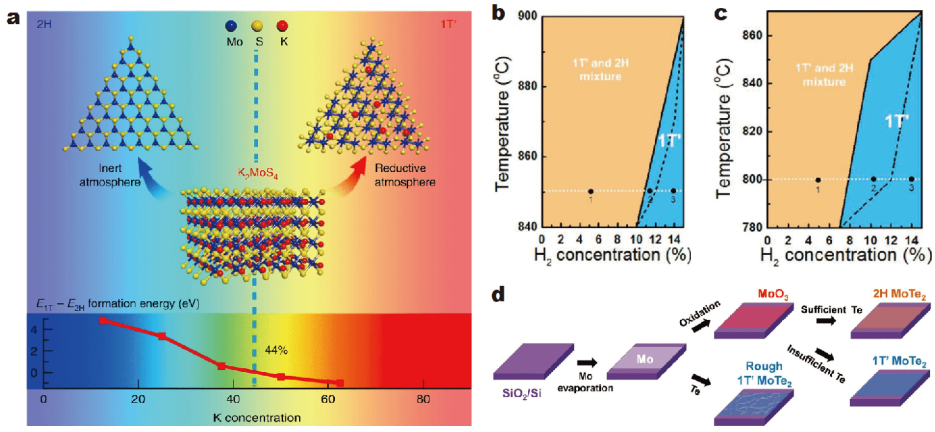

Figure 7 Phase-selective synthesis depending on precursor design. (a) Illustration of selective synthesis of 2H- or 1T′-MoS_2 under different atmospheres with K_2MoS_4 precursor. The inset plots at the bottom show the formation-energy difference between 1T′- and 2H-K_xMoS_2 as a function of K concentration. (b, c) Phase diagrams for the growth of MoS_2 using Rb_2MoS_4 and Cs_2MoS_4 precursor, respectively. Reproduced with permission from Ref. [119]. Copyright 2018, Springer Nature. (d) Illustration of the phase-selective growth process for 2H- and 1T′- $MoTe_2$ by using MoO_3 and Mo as precursors or tuning the Te flux with MoO_3 serving as precursor. Reproduced with permission from Ref. [121]. Copyright 2016, John Wiley and Sons.

selective synthesis has been utilized to achieve high phase purity and construct polymorphic heterostructures.

Precursor design

Precursor design plays an important role in the TMDs growth, because the precursors affect the reaction thermodynamically. As a demonstration, the controllable and large-scale synthesis of 2H-MoS_2 has been achieved [116–118], but there are still some challenges existing in the fabrication of metastable 1T (1T')-MoS_2 [33]. To stabilize the 1T' phase, Jiao *et al.* [119] prepared 1T'-MoS_2 by using K_2MoS_4 as Mo source. It is theoretically calculated that 1T'-K_xMoS_2 holds higher stability than 2H-K_xMoS_2 as the K concentration rises up to 44% (Fig. 7a). Other precursors, such as Cs_2MoS_4 and Rb_2MoS_4, can also be utilized to achieve the phase-selective synthesis of 1T'-MoS_2 (Fig. 7b and c). In addition, such a strategy is suitable to obtain 1T'-WS_2 [119] and 1T'-$MoSe_2$ [56]. Besides, precursor design can also be employed to the phase-selective synthesis of $MoTe_2$. Kong *et al.* [120] reported that the component of the Mo source was essential for the CVD growth of $MoTe_2$. The structure of $MoTe_2$ strongly relies on the Mo oxidation state, as well as the tellurization efficiency. Therefore, the phase-selective synthesis of pure 1T'- and 2H-$MoTe_2$ in CVD is realized by using Mo and MoO_3 as Mo precursors, respectively (Fig. 7d) [121]. Moreover, 1T'-$MoTe_2$ is predicted to be thermodynamically stable in the presence of certain mechanical stress [33]. In other words, when Mo foil serves as the precursor, a large stress may be generated during the formation of 1T'-$MoTe_2$, derived from the 380% increase of unit cell volume from Mo to $MoTe_2$. While MoO_3 acts as the precursor, the lower volume change (~47%) from MoO_3 to $MoTe_2$ can be released during the high-temperature growth, and then thermodynamically stable 2H-$MoTe_2$ without strain can be obtained. Furthermore, Te atomic flux has an extraordinary impact on the $MoTe_2$ phases. With a sufficient amount of Te, 2H-$MoTe_2$ is supposed to be obtained whereas 1T'-$MoTe_2$ is obtained in the insufficient Te supply (Fig. 7d). In addition, special precursor supplement, such as Mo nanoislands deposited on substrates, can also be used for the phase-selective synthesis of $MoTe_2$ [122].

In brief, there are two main strategies of precursor design to achieve the phase-selective synthesis of TMDs, including the metal precursor selection and the chalcogen flux regulation. Precursor design exerts a great influence on the synthesis at the aspect of both thermodynamics and dynamics, but it remains further understanding for the mechanism and the universality for group VB TMDs.

Temperature control

Temperature control is also an efficient approach to direct synthesis of expected TMD phases, which mainly relies on controlling the growth temperature. Different from the thermal treatment which achieves the target phase based on as-obtained samples, temperature control aims at directly synthesizing different phase by changing temperature without any post treatment. Furthermore, researchers prefer to determine the synthetic pathway based on some specific products with ground-state energy

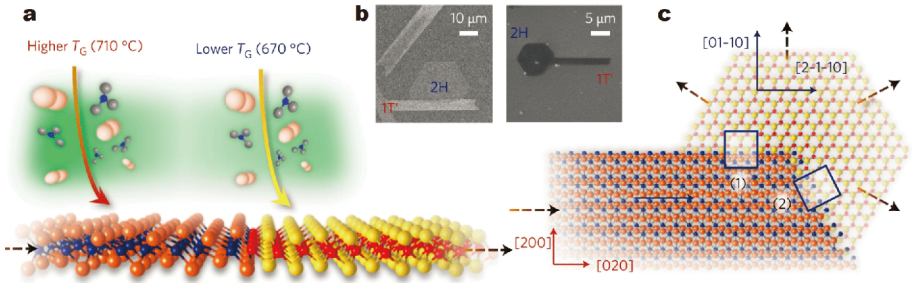

Figure 8 Phase-selective synthesis *via* temperature control. (a) Sequential growth of coplanar heteroepitaxy of 1T'/2H-$MoTe_2$ polymorphs. (b) SEM images of the 1T'-$MoTe_2$–2H-$MoTe_2$ heterostructures. (c) Schematics of the heteroepitaxial structure. Reproduced with permission from Ref. [57]. Copyright 2017, Springer Nature.

differences. Here we summarize the temperature control strategies in phase-selective synthesis for single phase crystals and polymorphic heterostructures, including direct vapor growth and van der Waals epitaxy.

Direct vapor growth of 2D polymorphs with distinct phase selectivity is an efficient but elusive way probably due to thermodynamic instability. Jo *et al.* [57] applied such an approach in the synthesis of $MoTe_2$ according to the relatively small difference in the ground-state energy between the 1T' and 2H phases. They used pure MoO_3 and Te as precursors, with NaCl applied to selectively stabilize different phase. As shown in Fig. 8a–c, when the growth temperature (T_G) reaches 710°C, the as-obtained rectangular- or trapezoidal-facet crystals are identified as 1T'-$MoTe_2$. At T_G=670°C, it mainly forms hexagonal or triangular facets corresponding to 2H-$MoTe_2$. At intermediate T_G (670°C<T_G<710°C), it tends to produce varied ratios of 1T'/2H mixtures. The researchers successfully demonstrated heteroepitaxial integration of few-layer $MoTe_2$ metal–semiconductor polymorphs within the same atomic planes which can be regarded as a promising atomic-scale electrical contact.

Van der Waals epitaxy is also a crucial way to grow various TMDs. Chen *et al.* [123] realized selective growth of specific phase WSe_2 at different temperatures *via* such a method. It is illustrated that a single-layer WSe_2 grown at a substrate temperature of 280°C exhibits a mixture of 1H and 1T' phases, and with the temperature climbing, the 1H phase plays a more dominant role until the 1T' phase totally disappears at growth temperature above 400°C. What's more, the 1T' phase prefers to grow at a lower temperature and at the growth temperature of 130°C all the products convert into 1T' phase. Monolayer 1T'-WSe_2 with a sizable quantum spin Hall (QSH) gap is conducive to further ambient-temperature spintronics, compared with 1T'-WTe_2 owning a smaller QSH gap. Besides, unlike exfoliated materials, the 1T'-WSe_2 film synthesized by molecular beam epitaxy (MBE) has a wider range of applications owing to the large-scale fabrication of devices such as topological field effect transistors (FETs).

In summary, phase-selective synthesis *via* temperature control is so facile and straightforward that attracts much attention. Just differing in practical steps, target phase TMDs, especially for metastable phases, can be obtained *via* the aforementioned methods, which offer a great platform for further studies and potential applications. In addition, taking temperature and percentages of precursors into account might make a difference.

Atmosphere regulation

Apart from the precursor design and temperature control, atmosphere also dynamically affect the phase-selective synthesis. As a reductive reagent, H_2 plays an important role in the TMDs growth as a kinetic effect [4]. Jiao *et al.* [119] reported that H_2 can accelerate the chemical transformation from K_2MoS_4 to K_xMoS_2. As shown in Fig. 9a, 1T'-2H mixed phase MoS_2 can be transformed to pure 1T' phase as the H_2 concentration ascends. Fig. 9b–d show the optical images of typical synthesis results corresponding to different H_2 concentrations marked with 1–3 in Fig. 9a. Owing to high H_2 concentrationsx, aforementioned K concentration can be kept in a relatively high value and the 1T' phase MoS_2 tends to be obtained. According to Fig. 9a, H_2 concentration shows a kinetic effect based on the particular precursor design and temperature control. Nevertheless, the growth of metastable phase TMDs is not likely to only depend on atmosphere regulation, because the carrier gas can only help with the dynamic process rather than the thermodynamic process. For TMD growth, H_2 is utilized to improve the reactivity of nonmetal precursors and regulate the expanding or etching along the TMD crystal edges. Therefore, atmosphere regulation can be an

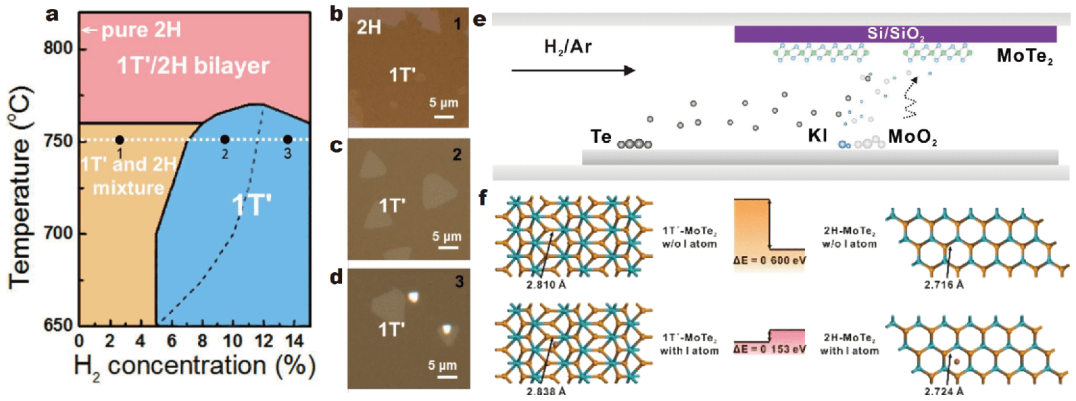

Figure 9 Atmosphere regulation and medium assistance for phase-selective synthesis. (a) Phase diagram of 1T' and 2H MoS_2. (b–d) The optical images of growth results corresponding to different H_2 concentrations marked with 1–3 in (a). Reproduced with permission from Ref. [119]. Copyright 2018, Springer Nature. (e) Schematic illustration of iodine-assisted 1T'-$MoTe_2$ CVD growth. (f) Mechanism of the stabilizing of the 1T' phase and the bond parameters change by iodine assistance. Reproduced with permission from Ref. [58]. Copyright 2017, American Chemical Society.

indirect and assistant strategy to improve the phase selectivity.

Medium assistance

During the TMDs growth, the volatility of precursors and intermediates is crucial for the CVD process. Initially presented by Eda *et al.* [124] and then developed by Liu *et al.* [32], medium assistance has become one of the most effective ways to fabricate TMDs. Halide assistance aims at producing volatile intermediates and improving the reactivity. Xu *et al.* [125] reported millimeter-scale 1T'-$MoTe_2$ single crystals by using KCl and NaCl as growth promoters. The halides react with Mo precursor to produce volatile MoO_2Cl_2 and $MoOCl_4$, and then these intermediates accelerate the reaction with Te. However, it may not uncover the reason why the metastable 1T' phase was obtained rather than the stable 2H phase of $MoTe_2$. Fu *et al.* [58] developed an iodine-assisted strategy to fabricate 1T'-$MoTe_2$. Fig. 9e shows the schematic illustration of the 1T'-$MoTe_2$ growth. KI is not only utilized to produce volatile MoO_2I_2, but also to stabilize the 1T' structure. As shown in Fig. 9f, the total energy of 1T'-$MoTe_2$ is calculated to be 0.600 eV higher than that of 2H-$MoTe_2$, while the energy of iodine-adsorbed 1T'-$MoTe_2$ is 0.153 eV lower than that of iodine-adsorbed 2H-$MoTe_2$. Furthermore, compared with 2H-$MoTe_2$, the larger bond length change of Mo–Te bonds in 1T'-$MoTe_2$ after the iodine-assistance may also help to stabilize the 1T' phase. Actually, in consideration of the different structures of TMDs, assisted media which can stabilize the internal lattice strain are essential to phase-selective synthesis for metastable TMDs.

SUMMARY AND OUTLOOK

Phase engineering of 2D TMDs is essential to both structural engineering and property modulation, which arouse worldwide concern. Enormous efforts have been made to develop phase engineering strategies with high efficiency and excellent controllability. To obtain specific phases of TMDs, it is necessary to develop controllable phase engineering strategies which are classified into the phase transition and phase-selective synthesis strategies. Phase transition can be achieved through intercalation, charge transfer, external irradiation, thermal treatment and stress induction, varying in efficiency, controllability and phase purity. Currently, phase-selective synthesis strategies, such as precursor design, temperature control, atmosphere regulation and medium assistance have been utilized to directly generate specific phase TMDs and heterostructures. Their excellent selectivity and high phase purity can promote further development of device construction and innovative discovery of physical phenomena.

In spite of the recent progress made in phase engineering, challenges still remain to be overcome. Initially, phase purity is vital to both the transformation behavior of structure and property and the controllable synthesis of TMDs with specific phases. The phase transition induced by lithium ion intercalation for MoS_2 exhibits a ~80% phase purity from 2H to 1T phase [119]. In addition, the impurities or the defects introduced during phase engineering process can also affect the phase purity. Secondly, the stability of the products is also an important issue. The as-obtained metastable phases may convert to the original stable ones. Hence, it is

necessary to stabilize the products by post-treating or introducing stabilizing media. However, such post treatments and nonvolatile stabilizing media would result in the unexpected doping or defects and even the sacrifice of intrinsic properties. Finally, phase engineering for other TMDs (e.g., group VB TMDs) or new phases still remain to be uncovered.

Phase engineering is acknowledged as a promising field for structural and property modulation, as well as the enrichment of the phase library of 2D TMDs. Actually, there may be distinct phases from the existing ones, which exhibit extremely special properties. We are convinced that phase engineering of 2D TMDs especially for the advanced phase-selective synthesis will further promote the expansion of 2D material family and the development of application technologies.

Received 8 December 2018; accepted 15 January 2019; published online 13 February 2019

1 Zeng M, Xiao Y, Liu J, *et al.* Exploring two-dimensional materials toward the next-generation circuits: from monomer design to assembly control. Chem Rev, 2018, 118: 6236–6296
2 Yang H, Kim SW, Chhowalla M, *et al.* Structural and quantum-state phase transition in van der Waals layered materials. Nat Phys, 2017, 13: 931–937
3 Cai Z, Liu B, Zou X, *et al.* Chemical vapor deposition growth and applications of two-dimensional materials and their heterostructures. Chem Rev, 2018, 118: 6091–6133
4 Li H, Li Y, Aljarb A, *et al.* Epitaxial growth of two-dimensional layered transition-metal dichalcogenides: growth mechanism, controllability, and scalability. Chem Rev, 2018, 118: 6134–6150
5 Han GH, Duong DL, Keum DH, *et al.* Van der Waals metallic transition metal dichalcogenides. Chem Rev, 2018, 118: 6297–6336
6 Tan C, Lai Z, Zhang H. Ultrathin two-dimensional multinary layered metal chalcogenide nanomaterials. Adv Mater, 2017, 29: 1701392
7 Zhang X, Cheng H, Zhang H. Recent progress in the preparation, assembly, transformation, and applications of layer-structured nanodisks beyond graphene. Adv Mater, 2017, 29: 1701704
8 Tan C, Cao X, Wu XJ, *et al.* Recent advances in ultrathin two-dimensional nanomaterials. Chem Rev, 2017, 117: 6225–6331
9 Sun L, Zheng J. Optical visualization of MoS_2 grain boundaries by gold deposition. Sci China Mater, 2018, 61: 1154–1158
10 Liu J, Cao H, Jiang B, *et al.* Newborn 2D materials for flexible energy conversion and storage. Sci China Mater, 2016, 59: 459–474
11 Iannaccone G, Bonaccorso F, Colombo L, *et al.* Quantum engineering of transistors based on 2D materials heterostructures. Nat Nanotechnol, 2018, 13: 183–191
12 Ali MN, Xiong J, Flynn S, *et al.* Large, non-saturating magnetoresistance in WTe_2. Nature, 2014, 514: 205–208
13 Costanzo D, Jo S, Berger H, *et al.* Gate-induced superconductivity in atomically thin MoS_2 crystals. Nat Nanotechnol, 2016, 11: 339–344
14 Xi X, Wang Z, Zhao W, *et al.* Ising pairing in superconducting $NbSe_2$ atomic layers. Nat Phys, 2015, 12: 139–143
15 Costanzo D, Zhang H, Reddy BA, *et al.* Tunnelling spectroscopy of gate-induced superconductivity in MoS_2. Nat Nanotechnol, 2018, 13: 483–488
16 Sohn E, Xi X, He WY, *et al.* An unusual continuous paramagnetic-limited superconducting phase transition in 2D $NbSe_2$. Nat Mater, 2018, 17: 504–508
17 Fei Z, Zhao W, Palomaki TA, *et al.* Ferroelectric switching of a two-dimensional metal. Nature, 2018, 560: 336–339
18 Bonilla M, Kolekar S, Ma Y, *et al.* Strong room-temperature ferromagnetism in VSe_2 monolayers on van der Waals substrates. Nat Nanotechnol, 2018, 13: 289–293
19 Wu S, Fatemi V, Gibson QD, *et al.* Observation of the quantum spin Hall effect up to 100 kelvin in a monolayer crystal. Science, 2018, 359: 76–79
20 Tang S, Zhang C, Wong D, *et al.* Quantum spin Hall state in monolayer 1T'-WTe_2. Nat Phys, 2017, 13: 683–687
21 Voiry D, Mohite A, Chhowalla M. Phase engineering of transition metal dichalcogenides. Chem Soc Rev, 2015, 44: 2702–2712
22 Ma Y, Kuc A, Jing Y, *et al.* Two-dimensional Haeckelite NbS_2: A diamagnetic high-mobility semiconductor with Nb^{4+} ions. Angew Chem Int Ed, 2017, 56: 10214–10218
23 Ma X, Guo P, Yi C, *et al.* Raman scattering in the transition-metal dichalcogenides of 1T'–$MoTe_2$, T_d–$MoTe_2$, and T_d–WTe_2. Phys Rev B, 2016, 94: 214105
24 Shirodkar SN, Waghmare UV. Emergence of ferroelectricity at a metal-semiconductor transition in a 1T monolayer of MoS_2. Phys Rev Lett, 2014, 112: 157601
25 Chhowalla M, Shin HS, Eda G, *et al.* The chemistry of two-dimensional layered transition metal dichalcogenide nanosheets. Nat Chem, 2013, 5: 263–275
26 Wilson JA, Yoffe AD. The transition metal dichalcogenides discussion and interpretation of the observed optical, electrical and structural properties. Adv Phys, 1969, 18: 193–335
27 Xu M, Liang T, Shi M, *et al.* Graphene-like two-dimensional materials. Chem Rev, 2013, 113: 3766–3798
28 Ataca C, Şahin H, Ciraci S. Stable, single-layer MX_2 transition-metal oxides and dichalcogenides in a honeycomb-like structure. J Phys Chem C, 2012, 116: 8983–8999
29 Zhang X, Lai Z, Ma Q, *et al.* Novel structured transition metal dichalcogenide nanosheets. Chem Soc Rev, 2018, 47: 3301–3338
30 Wang X, Song Z, Wen W, *et al.* Potential 2D materials with phase transitions: structure, synthesis, and device applications. Adv Mater, 2018, 499: 1804682
31 Wang J, Wei Y, Li H, *et al.* Crystal phase control in two-dimensional materials. Sci China Chem, 2018, 61: 1227–1242
32 Zhou J, Lin J, Huang X, *et al.* A library of atomically thin metal chalcogenides. Nature, 2018, 556: 355–359
33 Duerloo KAN, Li Y, Reed EJ. Structural phase transitions in two-dimensional Mo- and W-dichalcogenide monolayers. Nat Commun, 2014, 5: 4214
34 Cheng P, Sun K, Hu YH. Memristive behavior and ideal memristor of 1T phase MoS_2 nanosheets. Nano Lett, 2016, 16: 572–576
35 Lin C, Zhu X, Feng J, *et al.* Hydrogen-incorporated TiS_2 ultrathin nanosheets with ultrahigh conductivity for stamp-transferrable electrodes. J Am Chem Soc, 2013, 135: 5144–5151
36 Li LJ, O'Farrell ECT, Loh KP, *et al.* Controlling many-body states by the electric-field effect in a two-dimensional material. Nature, 2016, 529: 185–189
37 Chen P, Pai WW, Chan YH, *et al.* Emergence of charge density

waves and a pseudogap in single-layer $TiTe_2$. Nat Commun, 2017, 8: 516
38 Li L, Fang X, Zhai T, *et al.* Electrical transport and high-performance photoconductivity in individual ZrS_2 nanobelts. Adv Mater, 2010, 22: 4151–4156
39 Mleczko MJ, Zhang C, Lee HR, *et al.* $HfSe_2$ and $ZrSe_2$: Two-dimensional semiconductors with native high-κ oxides. Sci Adv, 2017, 3: e1700481
40 Tsipas P, Tsoutsou D, Fragkos S, *et al.* Massless dirac fermions in $ZrTe_2$ semimetal grown on InAs(111) by van der Waals epitaxy. ACS Nano, 2018, 12: 1696–1703
41 Fu L, Wang F, Wu B, *et al.* Van der Waals epitaxial growth of atomic layered HfS_2 crystals for ultrasensitive near-infrared phototransistors. Adv Mater, 2017, 29: 1700439
42 Mangelsen S, Naumov PG, Barkalov OI, *et al.* Large non-saturating magnetoresistance and pressure-induced phase transition in the layered semimetal $HfTe_2$. Phys Rev B, 2017, 96: 205148
43 Guo Y, Deng H, Sun X, *et al.* Modulation of metal and insulator states in 2D ferromagnetic VS_2 by van der Waals interaction engineering. Adv Mater, 2017, 29: 1700715
44 Ji Q, Li C, Wang J, *et al.* Metallic vanadium disulfide nanosheets as a platform material for multifunctional electrode applications. Nano Lett, 2017, 17: 4908–4916
45 Li J, Zhao B, Chen P, *et al.* Synthesis of ultrathin metallic MTe_2 (M = V, Nb, Ta) single-crystalline nanoplates. Adv Mater, 2018, 30: 1801043
46 Wang X, Lin J, Zhu Y, *et al.* Chemical vapor deposition of trigonal prismatic NbS_2 monolayers and 3R-polytype few-layers. Nanoscale, 2017, 9: 16607–16611
47 Han JH, Kim HK, Baek B, *et al.* Activation of the basal plane in two dimensional transition metal chalcogenide nanostructures. J Am Chem Soc, 2018, 140: 13663–13671
48 Calandra M. Phonon-assisted magnetic mott-insulating state in the charge density wave phase of single-layer 1T $NbSe_2$. Phys Rev Lett, 2018, 121: 026401
49 Yoshida M, Ye J, Zhang Y, *et al.* Extended polymorphism of two-dimensional material. Nano Lett, 2017, 17: 5567–5571
50 Wang X, Liu H, Wu J, *et al.* Chemical growth of 1T-TaS_2 monolayer and thin films: robust charge density wave transitions and high bolometric responsivity. Adv Mater, 2018, 30: 1800074
51 Shi J, Chen X, Zhao L, *et al.* Chemical vapor deposition grown wafer-scale 2D tantalum diselenide with robust charge-density-wave order. Adv Mater, 2018, 30: 1804616
52 Miller DC, Mahanti SD, Duxbury PM. Charge density wave states in tantalum dichalcogenides. Phys Rev B, 2018, 97: 045133
53 Fu L, Sun Y, Wu N, *et al.* Direct growth of MoS_2/h-BN heterostructures *via* a sulfide-resistant alloy. ACS Nano, 2016, 10: 2063–2070
54 Acerce M, Voiry D, Chhowalla M. Metallic 1T phase MoS_2 nanosheets as supercapacitor electrode materials. Nat Nanotechnol, 2015, 10: 313–318
55 Tongay S, Zhou J, Ataca C, *et al.* Thermally driven crossover from indirect toward direct bandgap in 2D semiconductors: $MoSe_2$ *versus* MoS_2. Nano Lett, 2012, 12: 5576–5580
56 Yu Y, Nam GH, He Q, *et al.* High phase-purity 1T'-MoS_2- and 1T'-$MoSe_2$-layered crystals. Nat Chem, 2018, 10: 638–643
57 Sung JH, Heo H, Si S, *et al.* Coplanar semiconductor–metal circuitry defined on few-layer $MoTe_2$ *via* polymorphic heteroepitaxy. Nat Nanotechnol, 2017, 12: 1064–1070
58 Zhang Q, Xiao Y, Zhang T, *et al.* Iodine-mediated chemical vapor deposition growth of metastable transition metal dichalcogenides. Chem Mater, 2017, 29: 4641–4644
59 Deng K, Wan G, Deng P, *et al.* Experimental observation of topological Fermi arcs in type-II Weyl semimetal $MoTe_2$. Nat Phys, 2016, 12: 1105–1110
60 Gao Y, Liu Z, Sun DM, *et al.* Large-area synthesis of high-quality and uniform monolayer WS_2 on reusable Au foils. Nat Commun, 2015, 6: 8569
61 Wang QH, Kalantar-Zadeh K, Kis A, *et al.* Electronics and optoelectronics of two-dimensional transition metal dichalcogenides. Nat Nanotechnol, 2012, 7: 699–712
62 Ma Y, Liu B, Zhang A, *et al.* Reversible semiconducting-to-metallic phase transition in chemical vapor deposition grown monolayer WSe_2 and applications for devices. ACS Nano, 2015, 9: 7383–7391
63 Zheng F, Cai C, Ge S, *et al.* On the quantum spin hall gap of monolayer 1T'-WTe_2. Adv Mater, 2016, 28: 4845–4851
64 Wang Y, Liu E, Liu H, *et al.* Gate-tunable negative longitudinal magnetoresistance in the predicted type-II Weyl semimetal WTe_2. Nat Commun, 2016, 7: 13142
65 Tongay S, Sahin H, Ko C, *et al.* Monolayer behaviour in bulk ReS_2 due to electronic and vibrational decoupling. Nat Commun, 2014, 5: 3252
66 Zhong HX, Gao S, Shi JJ, *et al.* Quasiparticle band gaps, excitonic effects, and anisotropic optical properties of the monolayer distorted 1T diamond-chain structures ReS_2 and $ReSe_2$. Phys Rev B, 2015, 92: 115438
67 Miró P, Ghorbani-Asl M, Heine T. Two dimensional materials beyond MoS_2: Noble-transition-metal dichalcogenides. Angew Chem Int Ed, 2014, 53: 3015–3018
68 Zhao Y, Qiao J, Yu Z, *et al.* High-electron-mobility and air-stable 2D layered $PtSe_2$ FETs. Adv Mater, 2017, 29: 1604230
69 Fu L, Hu D, Mendes RG, *et al.* Highly organized epitaxy of dirac semimetallic $PtTe_2$ crystals with extrahigh conductivity and visible surface plasmons at edges. ACS Nano, 2018, 12: 9405–9411
70 Py MA, Haering RR. Structural destabilization induced by lithium intercalation in MoS_2 and related compounds. Can J Phys, 1983, 61: 76–84
71 Yang D, Sandoval SJ, Divigalpitiya WMR, *et al.* Structure of single-molecular-layer MoS_2. Phys Rev B, 1991, 43: 12053–12056
72 Wang H, Lu Z, Xu S, *et al.* Electrochemical tuning of vertically aligned MoS_2 nanofilms and its application in improving hydrogen evolution reaction. Proc Natl Acad Sci USA, 2013, 110: 19701–19706
73 Qi Y, Xu Q, Wang Y, *et al.* CO_2-induced phase engineering: protocol for enhanced photoelectrocatalytic performance of 2D MoS_2 nanosheets. ACS Nano, 2016, 10: 2903–2909
74 Zhang J, Wu J, Guo H, *et al.* Unveiling active sites for the hydrogen evolution reaction on monolayer MoS_2. Adv Mater, 2017, 29: 1701955
75 Yamaguchi H, Blancon JC, Kappera R, *et al.* Spatially resolved photoexcited charge-carrier dynamics in phase-engineered monolayer MoS_2. ACS Nano, 2015, 9: 840–849
76 Kappera R, Voiry D, Yalcin SE, *et al.* Phase-engineered low-resistance contacts for ultrathin MoS_2 transistors. Nat Mater, 2014, 13: 1128–1134
77 Silbernagel BG. Lithium intercalation complexes of layered transition metal dichalcogenides: An NMR survey of physical properties. Solid State Commun, 1975, 17: 361–365

78 Tan C, Luo Z, Chaturvedi A, *et al.* Preparation of high-percentage 1T-phase transition metal dichalcogenide nanodots for electrochemical hydrogen evolution. Adv Mater, 2018, 30: 1705509
79 Tan C, Zhao W, Chaturvedi A, *et al.* Preparation of single-layer $MoS_{2x}Se_{2(1-x)}$ and $Mo_xW_{1-x}S_2$ nanosheets with high-concentration metallic 1T phase. Small, 2016, 12: 1866–1874
80 Zeng Z, Yin Z, Huang X, *et al.* Single-layer semiconducting nanosheets: high-yield preparation and device fabrication. Angew Chem Int Ed, 2011, 50: 11093–11097
81 Lai Z, Chaturvedi A, Wang Y, *et al.* Preparation of 1T'-phase $ReS_{2x}Se_{2(1-x)}$ (x= 0–1) nanodots for highly efficient electrocatalytic hydrogen evolution reaction. J Am Chem Soc, 2018, 140: 8563–8568
82 Fan X, Xu P, Zhou D, *et al.* Fast and efficient preparation of exfoliated 2H MoS_2 nanosheets by sonication-assisted lithium intercalation and infrared laser-induced 1T to 2H phase reversion. Nano Lett, 2015, 15: 5956–5960
83 Cheng Y, Nie A, Zhang Q, *et al.* Origin of the phase transition in lithiated molybdenum disulfide. ACS Nano, 2014, 8: 11447–11453
84 Yan S, Qiao W, He X, *et al.* Enhancement of magnetism by structural phase transition in MoS_2. Appl Phys Lett, 2015, 106: 012408
85 Zhao W, Ribeiro RM, Eda G. Electronic structure and optical signatures of semiconducting transition metal dichalcogenide nanosheets. Acc Chem Res, 2015, 48: 91–99
86 Yin Y, Han J, Zhang Y, *et al.* Contributions of phase, sulfur vacancies, and edges to the hydrogen evolution reaction catalytic activity of porous molybdenum disulfide nanosheets. J Am Chem Soc, 2016, 138: 7965–7972
87 Eda G, Yamaguchi H, Voiry D, *et al.* Photoluminescence from chemically exfoliated MoS_2. Nano Lett, 2011, 11: 5111–5116
88 Tan SJR, Abdelwahab I, Ding Z, *et al.* Chemical stabilization of 1T' phase transition metal dichalcogenides with giant optical Kerr nonlinearity. J Am Chem Soc, 2017, 139: 2504–2511
89 Sun L, Yan X, Zheng J, *et al.* Layer-dependent chemically induced phase transition of two-dimensional MoS_2. Nano Lett, 2018, 18: 3435–3440
90 Wang L, Xu Z, Wang W, *et al.* Atomic mechanism of dynamic electrochemical lithiation processes of MoS_2 nanosheets. J Am Chem Soc, 2014, 136: 6693–6697
91 Kan M, Wang JY, Li XW, *et al.* Structures and phase transition of a MoS_2 monolayer. J Phys Chem C, 2014, 118: 1515–1522
92 Wang X, Shen X, Wang Z, *et al.* Atomic-scale clarification of structural transition of MoS_2 upon sodium intercalation. ACS Nano, 2014, 8: 11394–11400
93 Zhang R, Tsai IL, Chapman J, *et al.* Superconductivity in potassium-doped metallic polymorphs of MoS_2. Nano Lett, 2016, 16: 629–636
94 Liu Q, Li X, He Q, *et al.* Gram-scale aqueous synthesis of stable few-layered 1T-MoS_2: Applications for visible-light-driven photocatalytic hydrogen evolution. Small, 2015, 11: 5556–5564
95 Liu Q, Li X, Xiao Z, *et al.* Stable metallic 1T-WS_2 nanoribbons intercalated with ammonia ions: the correlation between structure and electrical/optical properties. Adv Mater, 2015, 27: 4837–4844
96 Li Y, Duerloo KAN, Wauson K, *et al.* Structural semiconductor-to-semimetal phase transition in two-dimensional materials induced by electrostatic gating. Nat Commun, 2016, 7: 10671
97 Wang Y, Xiao J, Zhu H, *et al.* Structural phase transition in monolayer $MoTe_2$ driven by electrostatic doping. Nature, 2017, 550: 487–491
98 Kim S, Song S, Park J, *et al.* Long-range lattice engineering of $MoTe_2$ by a 2D electride. Nano Lett, 2017, 17: 3363–3368
99 Kang Y, Najmaei S, Liu Z, *et al.* Plasmonic hot electron induced structural phase transition in a MoS_2 monolayer. Adv Mater, 2014, 26: 6467–6471
100 Enyashin AN, Yadgarov L, Houben L, *et al.* New route for stabilization of 1T-WS_2 and MoS_2 phases. J Phys Chem C, 2011, 115: 24586–24591
101 Chen Y, Xi J, Dumcenco DO, *et al.* Tunable band gap photoluminescence from atomically thin transition-metal dichalcogenide alloys. ACS Nano, 2013, 7: 4610–4616
102 Lin YC, Dumcenco DO, Huang YS, *et al.* Atomic mechanism of the semiconducting-to-metallic phase transition in single-layered MoS_2. Nat Nanotech, 2014, 9: 391–396
103 Suh J, Tan TL, Zhao W, *et al.* Reconfiguring crystal and electronic structures of MoS_2 by substitutional doping. Nat Commun, 2018, 9: 199
104 Title RS, Shafer MW. Band structure of the layered transition-metal dichalcogenides: an experimental study by electron paramagnetic resonance on Nb-doped MoS_2. Phys Rev Lett, 1972, 28: 808–810
105 Zhu J, Wang Z, Yu H, *et al.* Argon plasma induced phase transition in monolayer MoS_2. J Am Chem Soc, 2017, 139: 10216–10219
106 Cho S, Kim S, Kim JH, *et al.* Phase patterning for ohmic homojunction contact in $MoTe_2$. Science, 2015, 349: 625–628
107 Chow PK, Jacobs-Gedrim RB, Gao J, *et al.* Defect-induced photoluminescence in monolayer semiconducting transition metal dichalcogenides. ACS Nano, 2015, 9: 1520–1527
108 Tosun M, Chan L, Amani M, *et al.* Air-stable n-doping of WSe_2 by anion vacancy formation with mild plasma treatment. ACS Nano, 2016, 10: 6853–6860
109 Park JC, Yun SJ, Kim H, *et al.* Phase-engineered synthesis of centimeter-scale 1T'- and 2H-molybdenum ditelluride thin films. ACS Nano, 2015, 9: 6548–6554
110 Keum DH, Cho S, Kim JH, *et al.* Bandgap opening in few-layered monoclinic $MoTe_2$. Nat Phys, 2015, 11: 482–486
111 Wang Z, Sun YY, Abdelwahab I, *et al.* Surface-limited superconducting phase transition on 1T-TaS_2. ACS Nano, 2018, 12: 12619–12628
112 Song S, Keum DH, Cho S, *et al.* Room temperature semiconductor–metal transition of $MoTe_2$ thin films engineered by strain. Nano Lett, 2016, 16: 188–193
113 Nayak AP, Pandey T, Voiry D, *et al.* Pressure-dependent optical and vibrational properties of monolayer molybdenum disulfide. Nano Lett, 2015, 15: 346–353
114 Voiry D, Goswami A, Kappera R, *et al.* Covalent functionalization of monolayered transition metal dichalcogenides by phase engineering. Nat Chem, 2014, 7: 45–49
115 Yang K, Wang X, Li H, *et al.* Composition- and phase-controlled synthesis and applications of alloyed phase heterostructures of transition metal disulphides. Nanoscale, 2017, 9: 5102–5109
116 Kang K, Xie S, Huang L, *et al.* High-mobility three-atom-thick semiconducting films with wafer-scale homogeneity. Nature, 2015, 520: 656–660
117 Najmaei S, Liu Z, Zhou W, *et al.* Vapour phase growth and grain boundary structure of molybdenum disulphide atomic layers. Nat Mater, 2013, 12: 754–759

118 Ju M, Liang X, Liu J, *et al.* Universal substrate-trapping strategy to grow strictly monolayer transition metal dichalcogenides crystals. Chem Mater, 2017, 29: 6095–6103
119 Liu L, Wu J, Wu L, *et al.* Phase-selective synthesis of 1T' MoS_2 monolayers and heterophase bilayers. Nat Mater, 2018, 17: 1108–1114
120 Zhou L, Xu K, Zubair A, *et al.* Large-area synthesis of high-quality uniform few-layer $MoTe_2$. J Am Chem Soc, 2015, 137: 11892–11895
121 Zhou L, Zubair A, Wang Z, *et al.* Synthesis of high-quality large-area homogenous 1T' $MoTe_2$ from chemical vapor deposition. Adv Mater, 2016, 28: 9526–9531
122 Yoo Y, DeGregorio ZP, Su Y, *et al.* In-plane 2H-1T' $MoTe_2$ homojunctions synthesized by flux-controlled phase engineering. Adv Mater, 2017, 29: 1605461
123 Chen P, Pai WW, Chan YH, *et al.* Large quantum-spin-Hall gap in single-layer 1T' WSe_2. Nat Commun, 2018, 9: 2003
124 Li S, Wang S, Tang DM, *et al.* Halide-assisted atmospheric pressure growth of large WSe_2 and WS_2 monolayer crystals. Appl Mater Today, 2015, 1: 60–66
125 Chen K, Chen Z, Wan X, *et al.* A simple method for synthesis of high-quality millimeter-scale 1T' transition-metal telluride and near-field nanooptical properties. Adv Mater, 2017, 29: 1700704

Acknowledgements This work was supported by the National Natural Science Foundation of China (21673161 and 21473124), the Science and Technology Department of Hubei Province (2017AAA114), and the Sino-German Center for Research Promotion (1400).

Author contributions Xiao Y, Zhou M, Liu J and Xu J wrote the manuscript; Fu L and Xiao Y developed the concept and revised the manuscript; Xiao Y prepared the figures; Xiao Y and Liu J classified and analyzed the reference papers. All authors participated in the general discussion.

Conflict of interest The authors declare no conflict of interest.

Yao Xiao received his BSc degree in chemistry from Wuhan University in 2016 and continued as a PhD candidate under the supervision of Prof. Lei Fu at the Institute of Advanced Studies at Wuhan University. His current scientific interest focuses on the special growing phenomena and electronics of 2D materials and heterostructures.

Mengyue Zhou received her BSc from Huazhong Agricultural University in 2017 and continued her studies as a master candidate under the supervision of Prof. Lei Fu at the College of Chemistry and Molecular Sciences at Wuhan University. Her current research interest is the controllable growth of two-dimensional material.

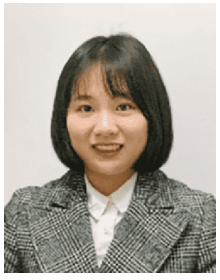

Jinglu Liu is pursuing her Bachelor's degree from the College of Chemistry and Molecular Science, Wuhan University. Her current research focuses on the synthesis of 2D transition metal dichalcogenide materials.

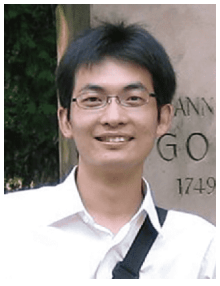

Lei Fu received his BSc degree in chemistry from Wuhan University in 2001. He obtained his PhD degree from the Institute of Chemistry, Chinese Academy of Sciences in 2006. Then he worked as a Director's Postdoctoral Fellow at the Los Alamos National Laboratory, Los Alamos, NM (2006–2007). Thereafter, he became an Associate Professor at Peking University. In 2012, he joined Wuhan University as a Full Professor. His current interest of research includes the controlled growth and novel property exploration of 2D atomic layer thin crystals.

二维过渡金属二硫族化合物的相工程

肖遥[1], 周梦月[2], 刘晶璐[2], 徐婧[2], 付磊[1,2*]

摘要 二维过渡金属二硫族化合物因其多样的原子排布和能带结构而备受关注. 除了热力学稳定的相之外, 许多亚稳态相的过渡金属二硫族化合物也表现出有趣的性质. 为了获得特定相的二维过渡金属二硫族化合物, 相工程策略(包括相转变和相选择合成)凸显的十分重要. 在本文中, 我们首先介绍了不同相的二维过渡金属二硫族化合物的结构和稳定性. 接着, 我们总结了多种相转变策略的详细过程和机理. 此外, 由于对过渡金属二硫族化合物相纯度的需求不断提升, 我们也展示了新型的相选择合成策略. 最后, 我们从相纯度和可控性两个方面指出二维过渡金属二硫族化合物相工程面临的挑战, 展望了相工程策略在可控获得高相纯度过渡金属二硫族化合物的前景. 这篇综述将促进二维过渡金属二硫族化合物及其他二维材料的可控相工程在基础研究和实际应用方面的发展.

